International Journal of Water Resources and Environmental Engineering Vol. 3(13), pp. 308-323, 8 December, 2011
Available online at http://www.academicjournals.org/IJWREE
DOI: 10.5897/IJWREE11.071
ISSN 1991-637X ©2011 Academic Journals

Full Length Research Paper

Thermosyphon solar water distiller of cement and aluminum absorber with auxiliary condenser

Mousa M. Mohamed* and Mostafa A. Abd El-Baky

Mechanical Power Engineering Department, Faculty of Engineering, Minufiya University, Shebin El-Kom, Egypt.

Accepted 27 October, 2011

Two modifications of solar water distillers using cement and aluminum absorbers are presented experimentally. The first modification uses separated condenser to purge vapor from the cement absorber distiller to increase the condensation, while second modification uses a plate thermosyphon charged with acetone installed on the bottom of the water basin in the aluminum absorber distiller to increase input energy to the distiller, thus increasing water vaporization and condensation. The optimum tilted angle of the glazing surface calculated to between 10 to 20° at latitude angle of 30°. The daily productivity of the cement absorber distiller was 2.08 L/ (m^2.day) and increased by percentage of 18% using the separated condenser and the overall efficiency being increased from 35% to more than 48%. For the aluminum absorber distiller the average daily productivity was 2.96 L/(m^2.day) and increased to 3.49 L/(m^2.day) using plate thermosyphon with the overall efficiency being increased from 50% to more than 65%.

Key words: Solar distiller, cement absorber, auxiliary condenser, aluminum absorber.

INTRODUCTION

Most human activities are intensively dependent on the water resources such as underground water, rains, lakes and rivers. However, rapid industrial growth and the population explosion all over the world have resulted in a large escalation of demand for fresh water. Add to this, the problems of pollution of rivers and lakes by industrial wastes and large amounts of sewage discharged (Kalogirou, 1997). While water covers about three-quarters of the earth' surface, only 3% of it is fresh water and not all of this limited quantity is suitable for drinking. Thus, water treatment is usually needed, and desalination is widely used for providing fresh water from brackish or seawater. Furthermore, supplying the required amount of potable water is already a problem in remote and arid areas which have limited supply of conventional energy, but have great potential for solar energy. Solar distillers based on renewable, safe, free and clean energy are a promising, cost effective solution. The production of fresh water using solar distillers has been presented in many studies (Abu-Jabal et al., 2001; John, 2003; Ali et al., 2005). Several types of solar distillers exist, the simplest of which is the single-basin type, but the yield of this distiller is in the range of 2 to 4 L/day per m^2 of distiller area. This type of distiller has the advantage of low installation costs but disadvantages of low efficiency, salt accumulation, and short lifetime (Schwarzer et al., 2001; Mailk et al., 1992; Shawaqfeh and Farid, 1995). Many generations of solar systems and distillers have been developed but only a very small number have been put into practice because of low efficiency and small amount of distilled water produced. A new approaches to enhance performance of solar desalination system was presented by Schwarzer et al. (2001) whereby the productivity of 25 L/day per m^2 was reached using such a system of heat recovery. Addition, solar distiller productivity was increased using a flat plate solar collector Zaki et al. (1983) and the maximum increase in the yield was up to 33% when the water is preheated in the collector. Tanaka and Nakataka (2004).

There have been recent works that investigated similar solar distillation systems using heat-pipe solar collector (Tanaka and Nakataka, 2004; Tanaka et al., 2004; 2005). They theoretically predicted that the optimum angle of the solar collector, and performed parametric investigation of design and operation conditions. The distiller is predicted to produce approximately 21.8 L/day per m^2 of distilled

*Corresponding author. E-mail: mousamohamed@yahoo.com.

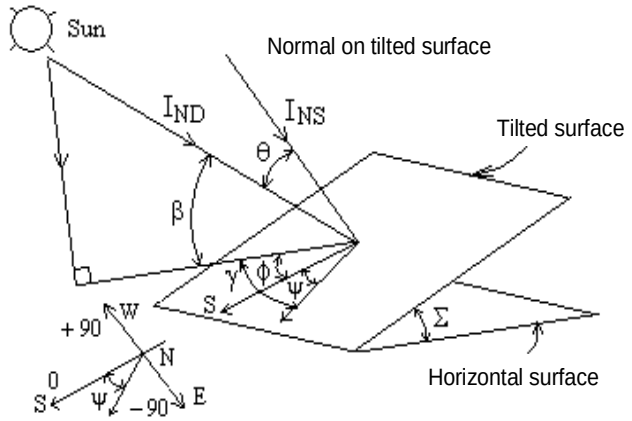

Figure 1. Direct solar radiation and incident normal component on tilted surface.

water, and the productivity is greater than that of bulky basin type distillers. Performance analysis of solar distiller coupled to a separated heat exchanger was presented (El-Bahi and Inan, 1999a). The separated condenser was used to purge water vapor to be condensed and the efficiency of the distiller was increased from 48% to more than 70%. The proposed solar distiller worked perfectly with daily yield of 7 L/day per m^2.

In this study, two modifications of solar water distiller using cement and aluminum absorber are presented experimentally. The first modification uses a separated condenser to purge water vapor from the cement absorber distiller to increase the condensation, while the second modification uses a plate thermosyphon charge with acetone installed on the bottom of the water basin in the aluminum absorber distiller to increase input energy to the distiller, thus increasing water vaporization and condensation. The effects of glazing surface tilted angle and orientation towards the south or the sun on the incident solar energy are also carried out.

Mathematical approach of solar radiation

The performance of a solar distiller is related to the surface azimuth angle or orientation, ψ, and surface tilt angle, Σ. To clarify the optimum tilt angle of solar collector at a certain site, the ASHRAE model (1981) has been used to estimate the normal direct solar radiation, I_{ND}, the normal component on the tilted surface I_{NS}, and solar incident angle θ, which is between the normal direct solar radiation and the normal component on the tilted surface as shown in Figure 1:

$$I_{ND} = A e^{-B/\sin\beta} \quad (1)$$

$$I_{NS} = I_{ND}\cos\theta \quad (2)$$

$$\theta = \cos^{-1}(\sin\beta\cos\Sigma + \cos\beta\cos\gamma\sin\Sigma) \quad (3)$$

where the solar plane azimuth angle $\gamma = \phi - \psi$, and solar azimuth angle ϕ. Thus, the global solar radiation I_G on the horizontal surface ($\Sigma=0$) is considered to be the sum of vertical components of the direct solar radiation and diffuse:

$$I_G = I_{ND}(\sin\beta + C) \quad (4)$$

Total solar radiation incident on the tilted surface with angle Σ is defined as,

$$I_{TS} = I_{NS} + I_{Ds} + I_{Rg} \quad (5)$$

where the diffused radiation I_{Ds} and the reflection from the earth surface I_{Rg} are defined as,

$$I_{Ds} = C I_{ND} F_{SS} \quad (6)$$

$$I_{Rg} = \rho_g F_{Sg} I_{ND}(\sin\beta + C) \quad (7)$$

Where:

$$F_{SS} = (1+\cos\Sigma)/2 \quad (8)$$

$$F_{Sg} = 1 - F_{SS} = (1-\cos\Sigma)/2 \quad (9)$$

Incorporating Equations 2 and 6-9 into Equation 5 yields:

$$I_{TS} = I_{ND}[\cos\theta + C F_{SS} + \rho_g F_{Sg}(\sin\beta + C)] \quad (10)$$

The solar radiation outside the atmosphere A, the constants, B, and C, and formulas of solar angles are explained in Appendix B, as illustrated in ASHRAE model (1981). A computer program was developed to implement Equations 1 to 10 with the formulas of solar angles to estimate the normal direct solar radiation I_{ND}, the total solar radiation incident on the tilted surface at various tilt angle Σ, and surface azimuth angle ψ. To validate the accuracy of the program, the global solar radiation was measured at Menoufiya University, Shebin El-kom, Egypt with EPPLEY radiometer (PSP) with data being taken every 15 min as shown in Figures 2 and 3. It can be seen that there is a regular variation from sunrise to sunset with peak radiation at noon, and the estimated values of global radiation are closed to the recorded data. It can be seen that the agreement in general is fairly good and the difference between measured and estimated global radiation, I_G^+ can be expressed by the following relation:

$$I_G^+ = (I_{G_{Estimated}} - I_{G_{Measured}}) \Big/ I_{G_{Measured}} \quad (11)$$

The standard deviation or root mean square (RMS) deviation was employed to estimate the relative error of I_G^+ as the following:

$$SD = \sqrt{\sum_{i=1}^{i=n} (I_{G,i}^+)^2 \Big/ n} \quad (12)$$

The percentage of deviation between the estimated global solar

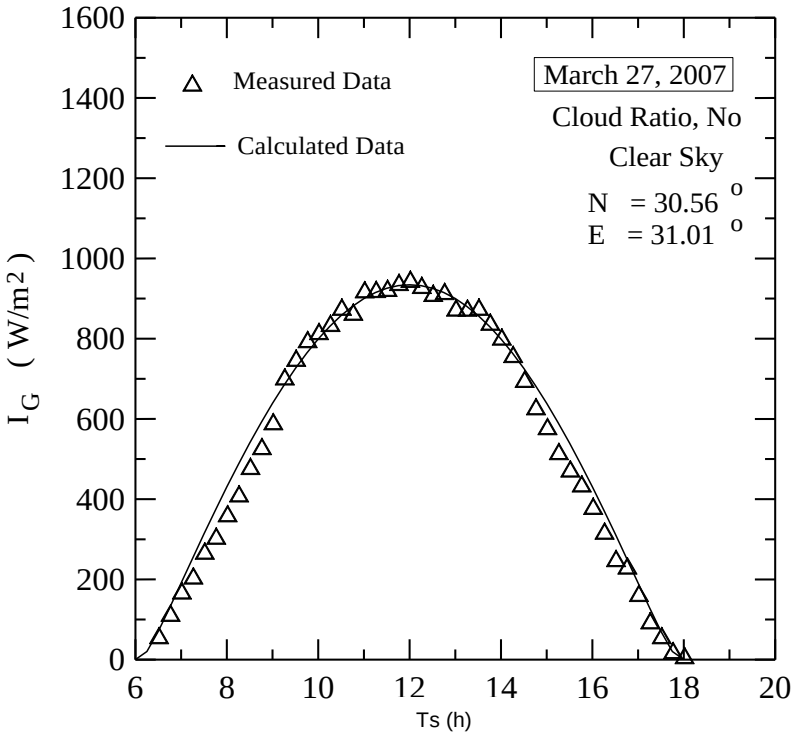

Figure 2. Shebin El-kom at N 30° 33\ E 31°, March 27, 2007.

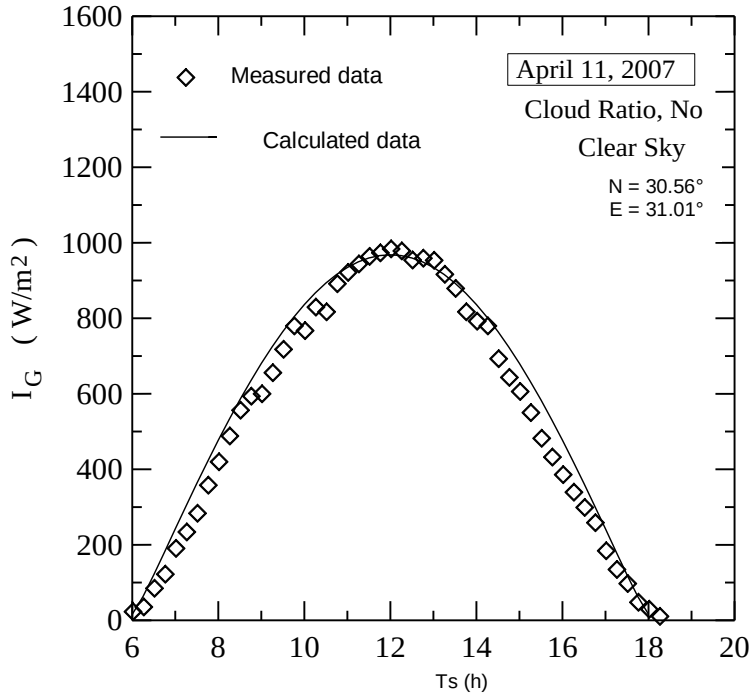

Figure 3. Shebin El-kom at N 30° 33\ E 31°, April 11, 2007.

radiations relative to the measured radiation is illustrated in Figure 4 It is observed that the agreement is satisfactory from 0900 to 1500. The percentage of deviation from sunrise to 0900 was positive (0 to 17%) because the estimated radiation was higher than the measured due to the effect of relative humidity in the morning. However, the percentage of deviation from 1500 to sunset was

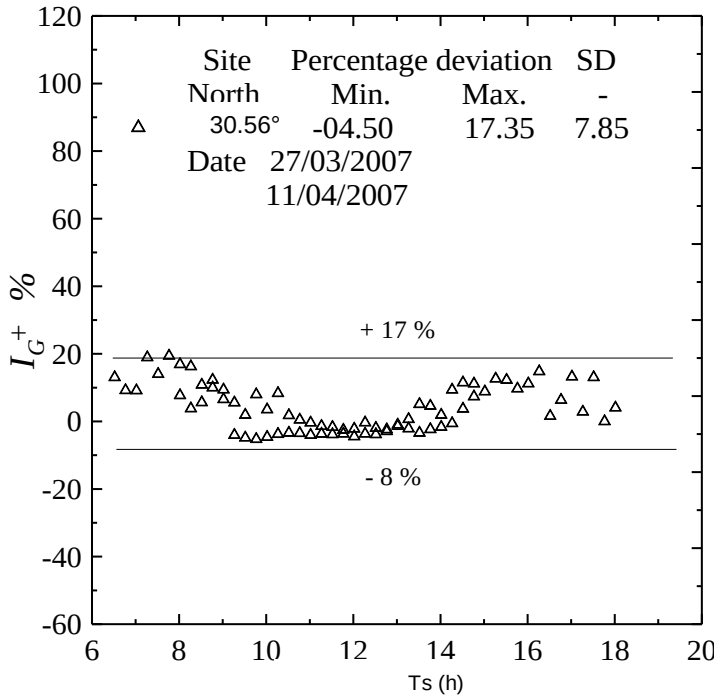

Figure 4. Percentage of deviation between estimated global solar radiation relative to the measured relation.

negative (in the range of -8 8 0%) because the measured radiation is higher than estimated radiation due to the increase of diffuse radiation. The low value of RMS deviation (5.02 to 7.85%) clearly proves that the proposed mathematical approach can be used for estimation of global solar radiation on horizontal and tilted surfaces at any location with a high level of confidence.

Based on this validation, the prepared computer program is considered an effective tool to study the effect of surface azimuth and tilt angle on the solar radiation incident on the tilted surface. The effect of tilt angle was investigated from horizontal ($\Sigma = 0°$) to vertical ($\Sigma = 90°$) surfaces, and surface azimuth from east to west in clock -wise step of 15° as shown in Figure 1. The optimum tilt angle was found to be 10 to 20° facing south, while the total solar incident on the tilted surface was maximum at noon, with $\Sigma = 20°$ as shown in Figure 5. Thus, tilted surface angle of 20° was used for the glazing surface of the solar distillers in this study.

Experimental apparatus

The experimental apparatus was constructed from two models as shown in Figures 6 to 7. The first model (Figure 6) was made using a wood basin with dimension of 1×1 ×0.15 m and 1.2 cm thickness. The inside faces of the wood basin were covered with cement layer of about 1.5 cm and divided into small channels of 4 cm depth and 8 cm width using a ceramic slab of 5 mm thickness. The channels were formed to decrease the amount of water deep in the basin and the thermal capacity of the distiller, and to increase the surface area of heat and mass transfer. The auxiliary condenser was made from galvanized steel of 0.25 mm thickness formed as a rectangular shape of 30 × 30 × 90 cm to increase the heat transfer area to accelerate the condensation of water vapor.

The second model (Figure 7) was made from aluminum sheet of 1 mm thickness and consists of a plate thermosyphon and a glazing solar distiller. The thermosyphon was constructed from two plates of aluminum of 1 × 2 m and the space between two plates was kept at 2 to 3 mm by making small webs on the upper plate. The four edges of the two plates welded together and examined before being charge with acetone. The dimensions of the glazing solar distiller are 1 × 1 × 0.15 m and it was fixed on the upper half of the thermosyphon. Parallel channels of 4 × 8 cm were formed in amphitheater shape to keep the water on the tilted surface and to decrease the thermal capacity of the distiller. The transparent surface was a white glass of 1×1 m and 3 mm thickness, which was sealed to prevent the escape of water vapor. The two models were inclined 20° to the horizontal surface, and all insides surfaces and channels were painted with a heavy black color to absorb solar radiation. Each model was mounted on a wooden frame, and the base and all side were thermally insulated.

The solar radiation incident on the tilted surface was measured using the EPPLEY radiometer which was fixed at the same level and tilt angle as the glazing surface. The yields or productivity of fresh water was measured by scale over 1 h. The thermosyphon was evacuated from the air and charged with one litter of acetone, which is equal to three quarter of the evaporator volume. The acetone was used as the working fluid because its boiling temperature is 57°C at atmospheric pressure and hence, is suitable for this application. Photos of the two models and solar radiometer are shown in Figure 8.

Thermal analysis of solar distiller

For each model, solar radiation hits the glazing surface of the solar distiller and the unglazed surface of the heat pipe plate. The solar radiation is transmitted through the glazing surface, and is absorbed by the black surfaces of the distiller. The black surfaces re-radiate long wave radiation that is directly absorbed by the water. The upper black surface of heat pipe plate absorbs solar radiation. A part of the heat is transferred to the surrounding by convection

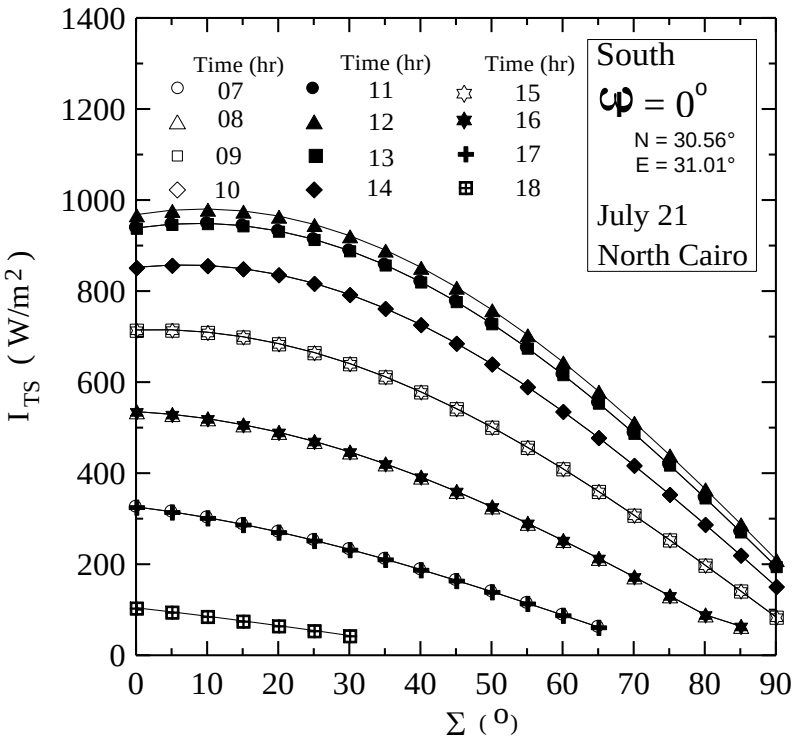

Figure 5. Effect of surface tilted angle on incident solar radiation to the south.

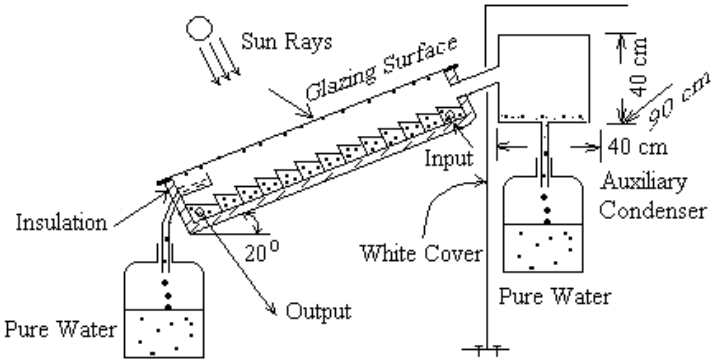

Figure 6. Layout of cement model solar distiller with auxiliary condenser.

and radiation, while the other part is transferred through the heat pipe plate. The liquid refrigerant absorbs heat, with evaporates, moving up to the upper half of heat pipe plate. The vapor refrigerant condenses at the inner surface and condensation heat is transferred by conduction to the water. The condensed refrigerant moves down, under gravity, to the lower part of the heat pipe plate, in order to repeat cycle. The water inside the passages of solar distiller warms and evaporates. The water vapor, which consists of moisture and dry air, moves freely up to the condensing surfaces. The temperature difference between water surface and condensing surfaces causes buoyancy force due to variation of partial vapor pressure.

Transmitted radiation and water heat gain

For a short time interval, a quasi-steady state condition could be considered for heat balance. The water heat gain in the distiller is the sum of transmitted solar radiation through the glazing surface and heat transferred through the heat pipe plate. The radiation transmitted through the glazing surface is dependent on the incident angle θ. As the base of the solar distiller and sides of the well are thermally insulated, the heat losses can be negligible, so the water heat gain can be estimated as:

$$H_w = A_{gl}\alpha_w\tau_{gl}I_{TS} + A_P(\alpha_P I_{TS} - q_{Pa}) \qquad (13)$$

where $q_{Pa,}$ is the sum of heat loss from the unglazed surface of the heat pipe plate to surrounding air by convection and radiation to the sky due to the following equations (Fath et al., 2003; Zeinab et al., 2005; Anil and Tiwari, 2006; Dunkle , 1961):

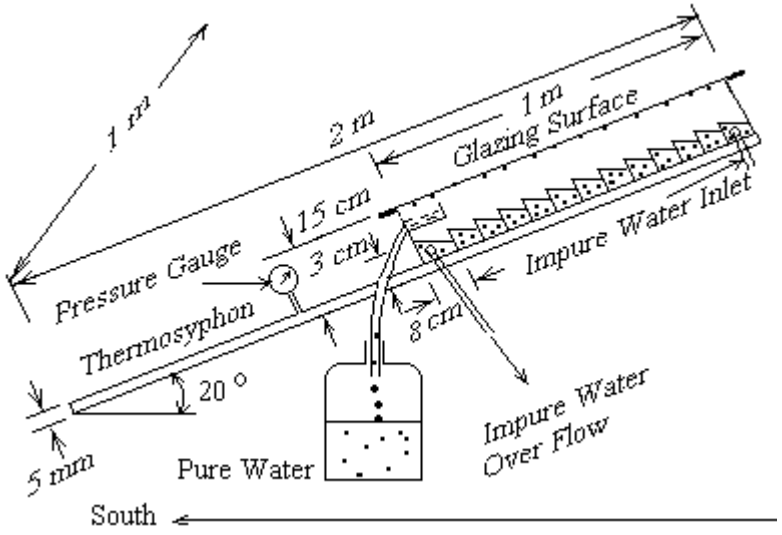

Figure 7. Layout of aluminum model solar distiller with thermosyphon.

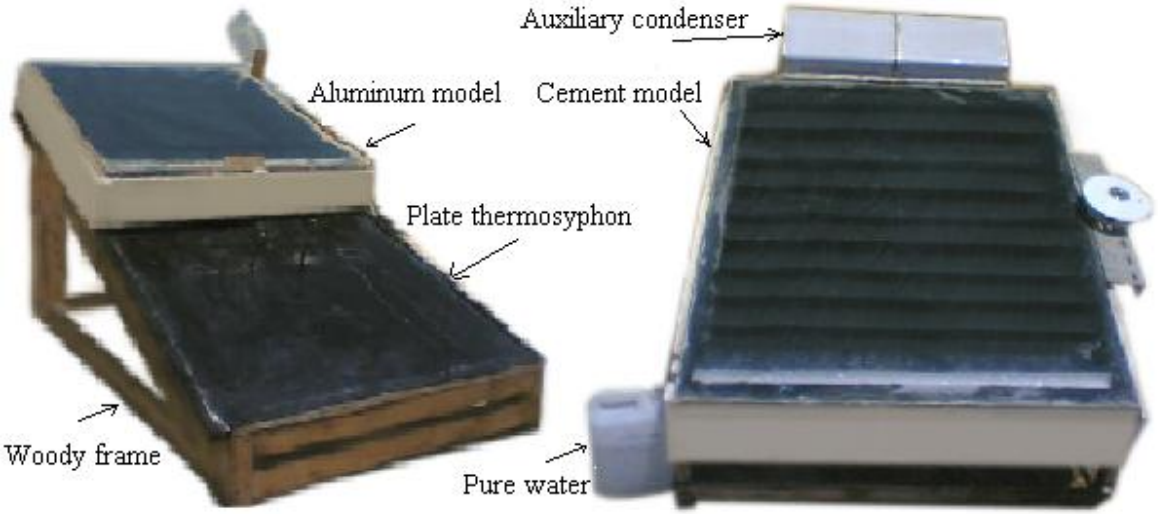

Figure 8. Photos of the cement and aluminum models.

$$q_{pa} = q_{pc} + q_{pr} = h_{pc}(T_p - T_a) + F_{p-s}\sigma[T_p^4 - T_{sky}^4] \quad (14)$$

where $T_{sky} = T_a - 10$

Water heat balance and distiller productivity

The absorbed heat by water in the distiller, the heat transmitted by convection, evaporation, radiation, and heat requiring for distiller system and feeding water can be expressed as (El-Bahi and Inan, 1999b; Duffie and Beckman, 1991):

$$H_w = A_w(q_{cw} + q_{rw}) + Q_{ew} + C_s\frac{dT_w}{dt} + FC_{pw}(T_w - T_a) \quad (15)$$

Where:

$$q_{cw} = 0.883\left[(T_w - T_{gi}) + \frac{(P_w - P_{wgi})(T_w + 273)}{(2.69P_a - P_w)}\right]^{\frac{1}{3}}(T_w - T_{gi}) \quad (16)$$

$$q_{rw} = F_{w-g}\sigma(T_w^4 - T_{gi}^4) \quad (17)$$

For the heat balance of water in steady state for the insulated well thermal, neglecting the distiller thermal capacity and feed water, the

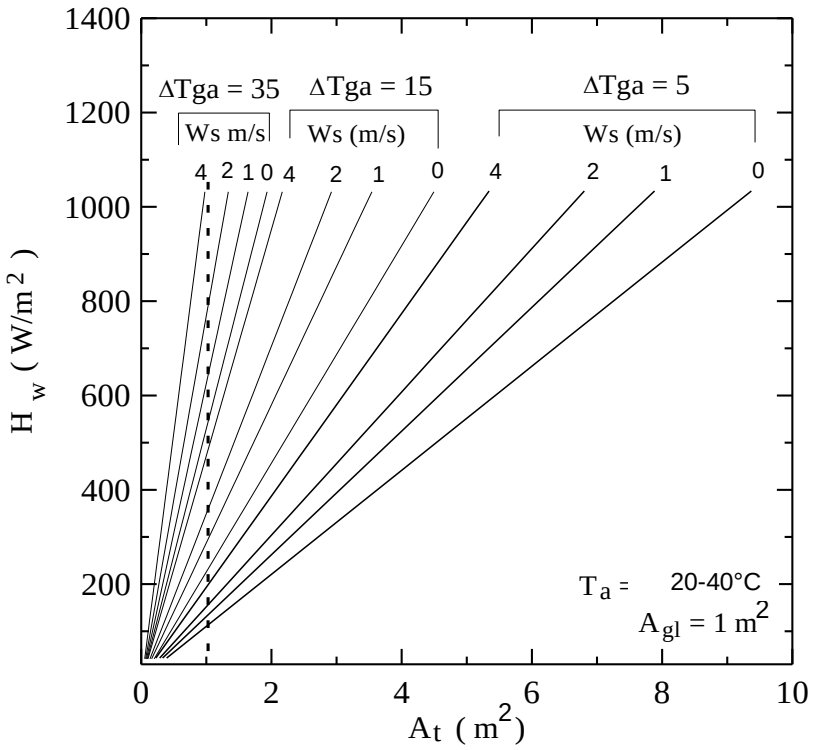

Figure 9. Heat transfer area for dissipation of heat to the surrounding air.

instantaneous productivity can be obtained as:

$$D_t = Q_{ew} / L_{wgi} \quad (18)$$

where $L_{wgi,}$ is the latent heat of evaporation at inner glazing surface temperature, while Q_{ew} is the transmitted heat by evaporation, which can be approximately calculated as (Elsayed et al., 1994):

$$q_{ew} = 6.1\times10^{-9}\left[(T_w - T_{gi}) + \frac{(P_w - P_{wgi})(T_w + 273)}{(2.69P_a - P_w)}\right]^{\frac{1}{3}}(P_w - P_{gi})\times L_{ww} \quad (19)$$

where $L_{ww,}$ is the latent heat of evaporation at water temperature in Jkg^{-1} and P_a is the atmospheric pressure. P_w and P_{wgi} are the saturation vapor pressure at water temperature and inner glazing surface temperature in Nm^{-2} respectively.

Glazing surface heat balance

The heat transfer from the glazing surface area to the surrounding is the sum of convection and radiation, which is equivalent to the water heat gain in the distiller and the absorbed heat in glazing surface.

$$A_t q_{ga} = H_w + A_{gl}\alpha_{gl} I_{TS} \quad (20)$$

Where:

$$q_{ga} = q_{gc} + q_{gr} \quad (21)$$

$$q_{gc} = h_{gc}(T_{go} - T_a) \quad (22)$$

$$q_{gr} = F_{g-s}\sigma(T_{go}^4 - T_{sky}^4) \quad (23)$$

The heat transfer area A_t from Equation 20 is required for heat dissipation to environment from the distiller to maximize productivity. The computer program was modified with the assumed clear sky solar radiation model to predict the distiller's instantaneous productivity for various wind speeds. Appendix A shows some important physical properties and parameters that were used to conduct the thermal analysis and calculation.

Theoretical dissipating heat transfer area and maximum productivity

The solar distiller thermal analysis in terms of heat transmitted to the distiller or water heat gain, wind speed, and temperature difference between the glazing surface to the surrounding air are illustrated in Figure 9. The calculations were made for glazing surface area of 1 m^2, surrounding air temperature of 20 to 40°C and wind speed of 0 to 4 m/s. The results showed that when the surrounding air temperature increased from 20 to 40°C, simulating air temperature change through daytime, the deviation range between 3 to 11%. In addition, the heat transfer area is dependent on the temperature difference between basin water and inner glazing surface and it decreases with increasing temperature difference between the water and glazing surfaces. A systematic decrease of heat transfer area with increasing wind speed and temperature differences between glazing surface and surrounding

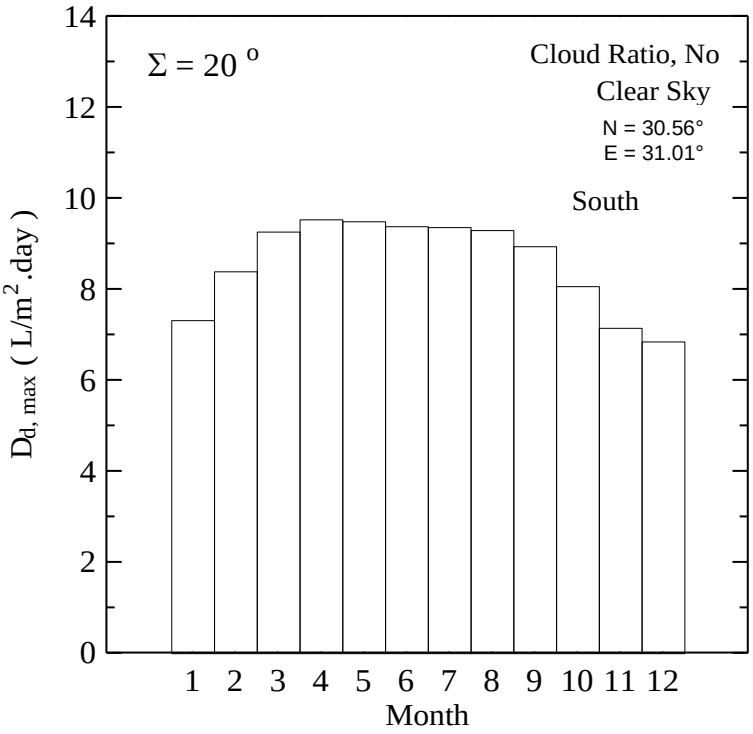

Figure 10. Theoretical maximum productivity per day at 21st day of each month.

air is observed, as illustrated in Figure 9. The dashed line in the graph at heat transfer area of 1 m^2 distinguishes the requirement for using an auxiliary surface. It can be seen that, towards left of dashed line, the glazing surface area is not sufficient for dissipating heat that is transmitted to the distiller and an auxiliary surface should be required. On the other hand, towards the right of the dashed line, the glazing surface area is sufficient for dissipating heat and obtaining maximum productivity. Figure 10 shows the maximum daily productivity for glazing surface area of 1 m^2, with the 21st day of each month being used as a reference. The calculation for the maximum daily productivity neglected radiation and convection from the water surface in the basin and losses from the basin's sides and base.

RESULTS AND DISCUSSION

The experimental program was conducted using both solar distiller models. The first model is the cement absorber distiller without and with the separated condenser which was orientated to the south, with the hourly productivities obtained as shown in Figure 11. It can be seen that the productivity increased gradually until noon, reaching the maximum thermal capacity of the distiller at about 1400. The experiments were repeated for 3 to 4 days to examine the data accuracy, with the measured values shown in Table 1. The daily productivity of the model was 2.08 L/ (m^2.day) without the condenser and 2.388 L/ (m^2.day) with the condenser, with a percentage increase about 18%. The surface area of the condenser used was 0.95 m^2. From the data in Figure 9, the measured wind velocity was less than 1 m/s and for ΔT_{ga}=15 K, the surface area of the condenser should be three times the glazing surface to increase the daily productivity for up to 90%. It is very important to note that the cement absorber model was used in this study because it is very cheep and easy to construct without any previous experience. Furthermore, it is easy to build using local materials such as bricks, cement and glass, besides wells, rivers, lakes and beaches to serve the people in arid and remote areas.

The second model was the aluminum absorber distiller, with the experiments conducted without the thermosyphon which orientated to south. Thereafter, the distiller was rotated every 30 min facing the sun until its shadow was underneath itself. In these experiments, the thermosyphon section was not charged with acetone and covered with thermal insulation to prevent solar energy from striking this section as shown in Table 2. The hourly productivities of the model are illustrated in Figure 12. The daily productivity was 2.96 L/ (m^2.day) when orientated to south and 4.39 L/ (m^2.day) when rotated to face the sun, with a percentage increase of 48.6%. The daily productivity of aluminum absorber facing the south is higher than the cement absorber by about 43.69%, because the aluminum absorber is allows the temperature of black surfaces and basin water is to be homogenous, resulting in accelerated water evaporation.

The plate thermosyphon was evacuated and charged with acetone. The daily productivity was 3.49 L/ (m^2.day)

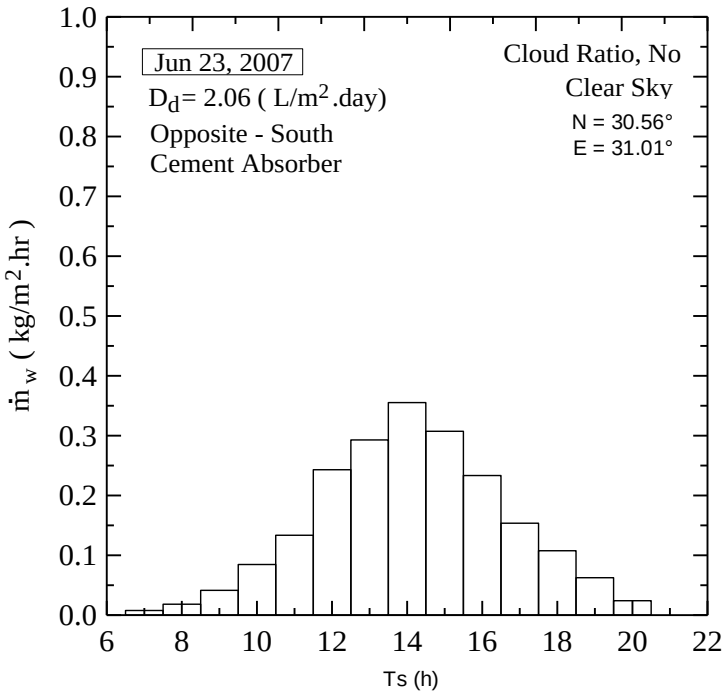

(a)

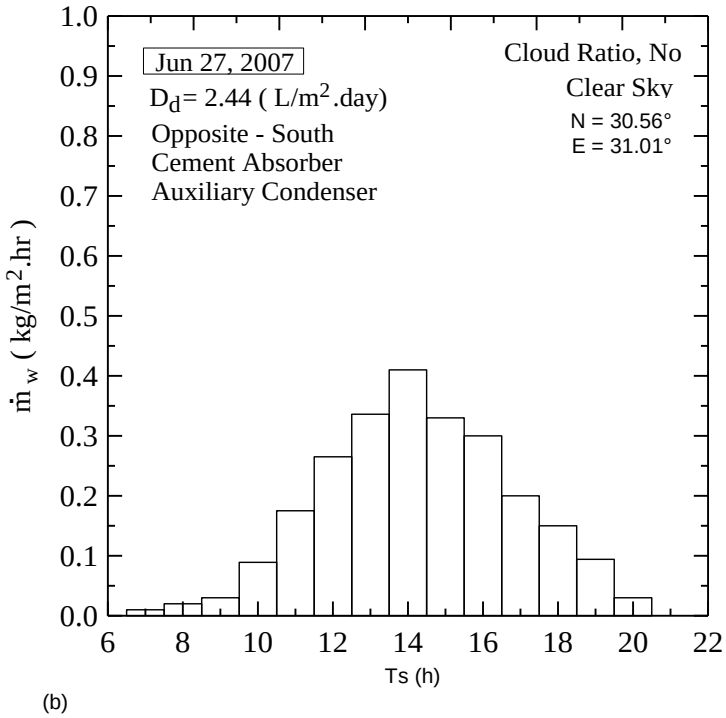

(b)

Figure 11. Hourly productivity of the cement model: (a) without and (b) with the condenser.

when orientated to south as shown in Figure 13. The daily productivity increased by about 18% compared to the distiller without thermosyphon. If the thermosyphon distiller was orientated facing the sun and its position changed every 30 min so that its shadow underneath itself, it possible that the daily productivity will increase up to 5.2 L/ (m^2.day).

Each distillers' overall efficiency is dependent on incident solar energy and is the ratio between solar energy utilized for water evaporation and solar radiation

Table 1. Hourly and daily productivities of the cement absorber model with and without the condenser.

Cement absorber	Date 2007	Daily productivity L/(m^2.day)	Average productivity L/(m^2.day)	Percentage increase (%)
Facing south without condenser	Jun 23	2.06	2.077	–
	Jun 24	2.10		
	Jun 25	2.07		
Facing south with condenser	Jun 27	2.44	2.388	18.7 %
	Jun 28	2.42		
	Jun 30	2.34		
	July 01	2.35		

Table 2. Hourly and daily productivities of the aluminum absorber model without and with the thermosyphon.

Aluminum absorber	Date 2007	Daily productivity L/(m^2.day)	Average productivity L/(m^2.day)	Percentage increase
Facing south without thermosyphon	Jun 30	2.97	2.955	–
	July 01	2.95		
	July 02	2.98		
	July 03	2.92		
Facing the sun without thermosyphon	July 04	4.46	4.39	48.6
	July 05	4.32		
Facing south with thermosyphon	July 07	3.46	3.487	18
	July 08	3.48		
	July 09	3.52		

incident on the glazing surface as,

$$\eta = \frac{\dot{m}_w \times LT}{H_s} \qquad (24)$$

The overall efficiencies of the studied cases are compared in Figures 14 to 16. Obviously, the distillers' efficiency increased with increasing solar energy until noon, but continued to increase because of the thermal capacity of the distiller and energy stored in the black surfaces and basin water. It is found that the efficiency of the cement absorber with condenser is higher than without condenser by about 5%, as shown in Figure 14. For the aluminum absorber, the efficiency is higher than cement absorber by about of 15%, as shown in Figure 15. For the aluminum absorber, the efficiency when using the thermosyphon was higher by about 8% as illustrated in Figure 16. However, when the aluminum absorber is continuously rotated to face the sun, the efficiency was increased by about 18%. From these results, the two modifications of condenser in the cement absorber and the thermosyphon in the aluminum absorber, resulted in the productivity being increased by about 18% and overall efficiency by about 5 to 8%.

Conclusions

An experimental study was performed to investigate the productivity and efficiency of solar water distiller using cement and aluminum absorbers.

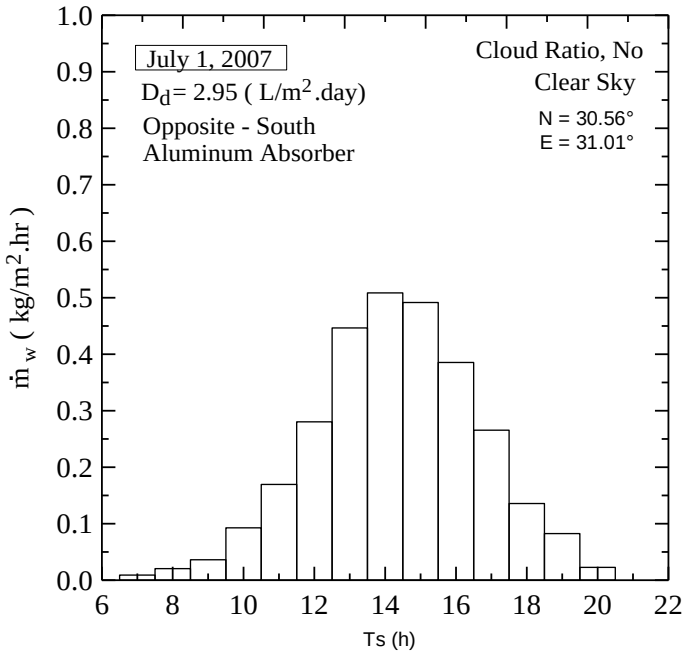

(a)

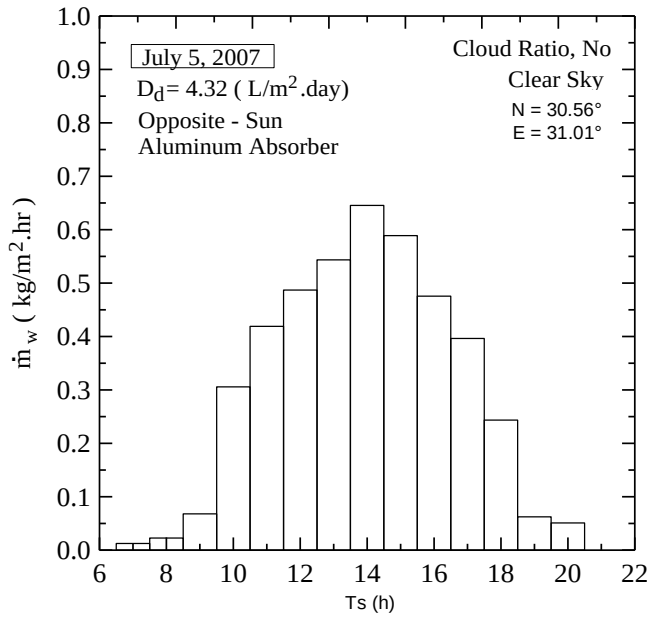

(b)

Figure 12. Hourly productivity of the aluminum model without thermosyphon facing: (a) the south (b) the sun.

Two modifications were used to enhance the productivity of the distillers. For the cement absorber, an auxiliary condenser was used to purge the water vapor to increase productivity. For the aluminum absorber, a thermosyphon charged with acetone was used to enhance the heat transfer underneath the water in the basin to increase evaporation and productivity. The results are summarized as:

1) The optimum tilted angle was calculated and it was found between 10 to 20° at latitude angle of 30°.
2) The average daily productivity of the cement absorber distiller orientated facing the south was 2.08 L/ (m^2.day) with overall efficiency of 38%. The productivity was increased to 2.39 L/ (m^2.day) with overall efficiency of45% when using the auxiliary condenser, with a

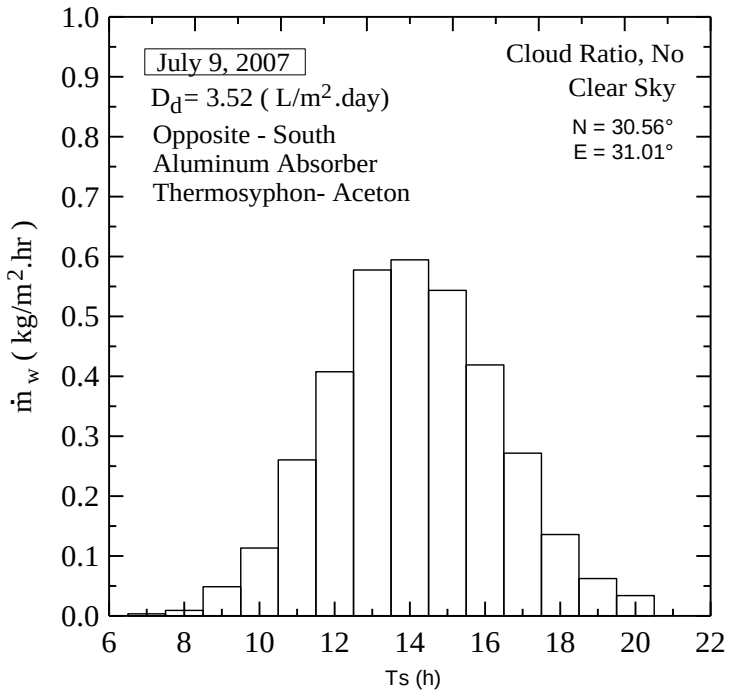

Figure 13. Hourly productivity of the aluminum model with thermosyphon.

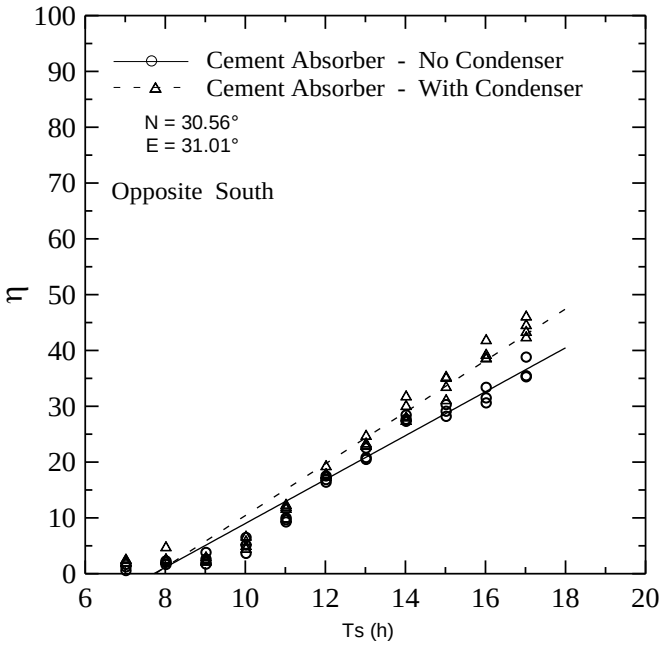

Figure 14. Cement absorber distillers' efficiencies with and without the condenser.

percentage of increase of 18% .

3) For the aluminum absorber orientated facing the south, the average daily productivity was 2.96 L/ (m^2.day) with overall efficiency of 50%. When the thermosyphon was used, the productivity obtained was 3.49 L/ (m^2.day) with overall efficiency up to 65%, with a percentage of increase of 18%.

4) For the aluminum absorber without the thermosyphon

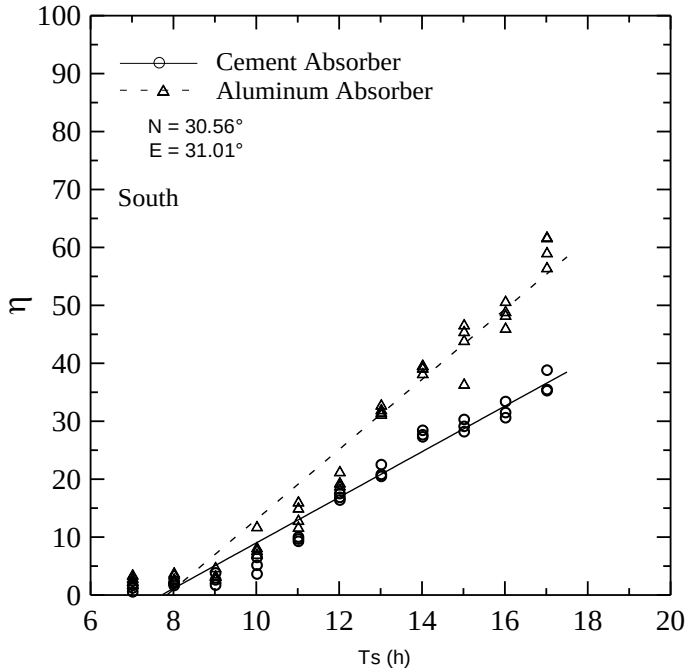

Figure 15. Cement and aluminum absorber distillers' efficiencies.

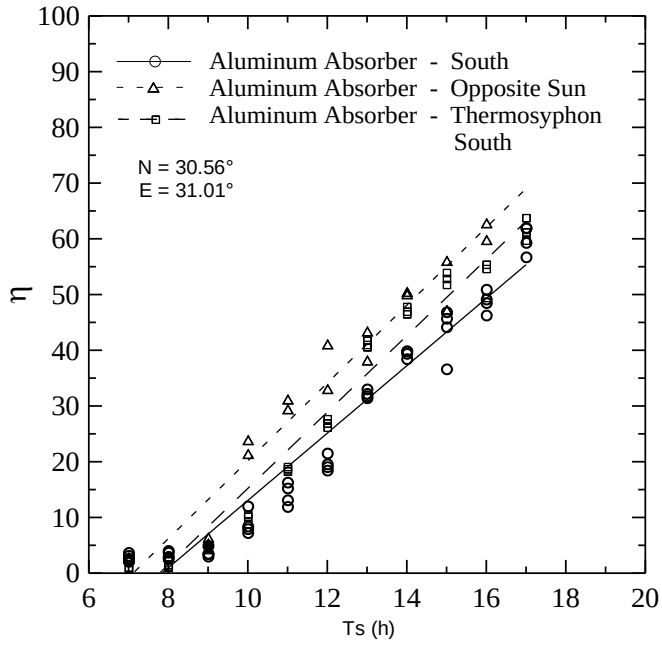

Figure 16. Aluminum distillers' efficiencies facing south and sun.

which was positioned with respect to the direction of the sun, the average daily productivity was attained to 4.39 L/ (m^2.day) with overall efficiency of 65%.

Nomenclature: A, Solar radiation intensity outside atmosphere (Wm^{-2}); A_P, Unglazed area of plate heat pipe to air (m^2); A_{gl}, Glazing surface area (m^2); A_w, Water surface area (m^2); A_t, Heat transfer area (m^2); B, Weakness atmospheric factor of solar radiation (-);C Diffuse radiation factor (-);C_s Distiller thermal capacity (JK^{-1}); C_{pw} Water specific heat ($Jkg^{-1}K^{-1}$); D_d Daily ditillate ($Lm^{-2}day^{-1}$); D_t distiller rate or productivity (kgs^{-1}); F, Feed,

water flow rate (Kgs^{-1}); F_{SS}, Angle factor between tilted surface and sky (-);F_{Sg}, Angle factor between tilted surface and ground surface (-);*H,* Solar hour angle (^{o}); H_s, Measured solar radiation incident on glazing surface (Wm^{-2}); H_W, Water heat gain (W); *h,* Heat transfer coefficient ($Wm^{-2}K$); h_{cw}, Convective heat transfer coefficient from water to glass ($Wm^{-2}K$); h_{ew}, Evaporative heat transfer coefficient ($Wm^{-2}K$); I_G, Global solar radiation on horizontal surface (Wm^{-2}); I_{ND}, Normal direct solar radiation intensity (Wm^{-2}); I_{NS}, Normal component of solar radiation on the tilted surface (Wm^{-2}); I_{TS}, Total solar radiation incident on the tilted surface (Wm^{-2}); L, Latitude angle of location (^{o}); L_g, Longitude angle of location (^{o}); LT, Latent heat of evaporation (Jkg^{-1}); $\dot{m}_w$ Hourly productivity ($kgm^{-2}hr^{-1}$); n, Day number from first of January (-);P_a, Atmospheric pressure (Nm^{-2}); P_w, Saturated vapor partial pressure at water temperature (Nm^{-2}); P_{wgi}, Saturated vapor partial pressure at inner glass temperature (Nm^{-2}); S, Solar beam angle to south (^{o}); T, Temperature (K); T_S, Solar time (hr); T_C, Local time of selected location (hr); T_{ZN}, Time zone longitude angle of selected location (^{o}); W, Solar beam angle to west (^{o}); W_S, Wind speed (ms^{-1}); Z, Solar beam angle with vertical (^{o}); Σ, Tilted surface angle (^{o}); α, Absorbtivity (-);β, Solar altitude angle (^{o}); ε, Emissivity (-); δ, Solar declination angle (^{o}); ϕ, Solar azimuth angle (^{o}); γ, Solar plan azimuth angle (^{o}); η, Distiller efficiency (^{o}); θ, Solar incident angle; ρ_g, Reflection factor form earth surface (^{o}); σ, Stefan – Boltzmann constant ($Wm^{-2}K^{-4}$); τ, Transmitivity (-);ψ, Surface azimuth angle.

Subscript: *A,* environment; *ds,* diffuse; *cw,* convective water*; ew,* evaporation water; *gl,* glass; *gc,* glass convection to air;
Gi, inner surface of glass; *go,* outer surface of glass; *gr,* radiation from out surface glass; *o,* environment; *p,*Plate; *pa,* plate to air;
Pc, plate convection to air; *pr,* plate radiation to sky; *Rg,* reflection from earth surface; *sky,* sky temperature;*W,* water; *cw,* convection from water surface; *ew,* evaporation from water surface; *rw,* radiation from water surface.

REFERENCES

Abu-Jabal M, Kamiya I, Narasaki Y (2001). Proving test for a solar-powered desalination system in Gaza-Palestine, Desalination, 1137: 1-6.

Ali AB, Ahmad AA-H, Imad AES, Mohammad ZO (2005). A Solar Distiller Augmented with a flat-plate collector, Desalination, 172: 227-234.

Anil Kr T, Tiwari GN (2006). Effect of water depth on heat and mass transfer in a passive solar distiller: in summer climatic condition, Desalination 195: 78-94.

ASHRAE (1981). Handbook of fundamentals, American Society of Heating, refrigeration and Air conditioning Engineers, Atlanta, W.S.A.

Duffie JA, Beckman WA (1991). Solar Engineering of Thermal Processes, 2nd ed. New York, Wiley Inter-science.

Dunkle RV (1961). Solar water didistilleration, the roof type distiller and multiple effect diffusion distiller, International Developments in Heat Transfer, ASME, Proc. International Heat Transfer, Part V, University of Colorado, p. 895.

El-Bahi A, Inan D (1999a). A solar distiller with minimum inclination coupled to an outside condenser, Desalination, 123: 79-83.

El-Bahi A, Inan D (1999b). Analysis of a parallel double glass solar distiller with separate condenser, Renewable Energy, 17: 509-521.

Elsayed MM, Taha IS, Sabbagh JA (1994). Design of Solar Thermal System, Scientific Publishing Center, King Abdulaziz University, Saudi Arabia, 1st Edition, p. 194.

Fath HES, El-Samanoudy M, Fahmy K, Hassabou A (2003). Therma-economic analysis and comparison between pyramid-shaped and single-slop solar distiller configurations, Desalination, 159: 69-79.

John W (2003). A plastic solar water purifier with high output, Solar Energy,75: 433-437.

Kalogirou S (1997). Survey of solar desalination system and system selection, Energy, 22: 1 69-181.

Klemens S (2003). Modular solar thermal desalination system with flat plate collector, RIO 3 – World Climate & Energy Event, 1-5 December 281-286, Rio de Janeiro, Brazil.

Mailk MAS, Tiwari GN, Kumar A, Sodha MS (1992).Solar didistilleration-a practical study of a wide range of distillers and their optimum design, construction and performance, Pergamon Press.

Schwarzer K, Vieira ME, Faber C, Mueller C (2001). Solar thermal desalination system with heat recovery, Desalination, 137: 23-29.

Shawaqfeh AT, Farid MM (1995). New development in the theory of heat and mass transfer in solar distillers, Solar Energy, 55(6): 527-535.

Tanaka H, Nakataka Y (2004). A vertical multiple-effect diffusion-type solar distiller coupled with a solar collector, Desalination, 160: 195-205.

Tanaka H, Nakatake Y, Tanaka M (2005). Indoor experiments of the vertical multiple-effect diffusion-type solar distiller coupled with a heat-pipe solar collector, Desalination, 177: 291-302.

Tanaka H, Nakatake Y, Watanabe K (2004). Parametric study on a vertical multiple-effect diffusion-type solar with a heat-pipe solar collector, Desalination, 171: 243-255.

Tiwari GN, Singh HN, Rajesh T (2003). Present status of solar distillation, 75(5): 367-373.

Zaki GM, Dali TE, Shafie HE (1983). Improved performance of solar distiller, proc. First Arab Int. Solar Energy Conf., Kuwait, pp. 331-335.

Zeinab S, Abdel R, Ashraf L (2005). Imporoving the performance of solar desalination systems, Renewable Enegry, 30: 1955-1971.

Appendix A. Some physical properties and parameters used to conduct the thermal analysis (20 to 22).

A_{gl} = 1 m^2	A_P = 1 m^2	A_w = 1.064 m^2	σ = 5.669×10^{-8} $Wm^{-2}K^{-4}$	
α_P = 0.97	α_w = 0.89	ε_g = 0.89	ε_p = 0.97	
ε_w = 0.96	ρ_g = 0.1			
h_{gc} = 5.61+3.924×W_S (Wind speed in m/s), $Wm^{-2}K^{-1}$				
h_{pc} = 6.18+4.284×W_S (Wind speed in m/s), $Wm^{-2}K^{-1}$				

$$F_{g-s}=[(1-\varepsilon_g)/\varepsilon_g+1/F_{SS}]^{-1},\ F_{p-s}=[(1-\varepsilon_p)/\varepsilon_p+1/F_{SS}]^{-1},\ F_{w-g}=[1/\varepsilon_w+1/\varepsilon_g-1]^{-1}$$

	c_o	c_1	c_2	c_3	c_4
$f(\theta)$	$\alpha_{gl},\rho_{gl},\tau_{gl}=c_o+c_1\theta+c_2\theta^2+c_3\theta^3+c_4\theta^4$, θ in degree.				
α_{gl}	0.0389495	0.00138832	-6.97256×10^{-5}	1.36745×10^{-6}	-8.75696×10^{-9}
ρ_{gl}	0.0833039	-0.00394181	2.90771×10^{-4}	-7.01009×10^{-6}	6.04023×10^{-8}
τ_{gl}	0.877747	0.00255349	-2.21046×10^{-4}	5.64265×10^{-6}	-5.16454×10^{-8}
$f(T)$	$L_w,P_v=c_o+c_1T+c_2T^2+c_3T^3+c_4T^4$, T in Kelvin.				
L_w	11491.7	-105.76	0.47722	-9.72101×10^{-4}	7.37019×10^{-7}
P_v	5.98167×10^6	-83911.7	443.553	-1.04794	9.34586×10^{-4}

Appendix B. Constant *A*, *B* and *C* at the 21 of every month from *ASHRAE,* (1981) (15).

Date	A (W/m^2)	B	C	Date	A (W/m^2)	B	C
January	1230	0.142	0.058	July	1085	0.207	0.136
February	1214	0.144	0.060	August	1107	0.201	0.122
March	1185	0.156	0.071	September	1151	0.177	0.092
April	1135	0.180	0.097	October	1192	0.160	0.073
May	1103	0.196	0.121	November	1220	0.149	0.063
June	1088	0.205	0.134	December	1233	0.142	0.057

Definition and formulas of sun and surface angles from *ASHRAE,* (1981) (15).

Angle	Formula
Solar declination angle	$\delta = 23.45 \frac{\pi}{180} \sin\left[2\pi \frac{(284+n)}{365}\right]$
Solar beam angle with vertical	$Z = \cos^{-1}(\sin L \sin\delta + \cos\delta \cos H \cos L)$
Solar altitude angle	$\beta = \pi/2 - Z$
Solar hour angle	$H = 15 \frac{\pi}{180}(T_S - 12)$
Solar time	$T_S = T_C + Et + \frac{4}{60}(T_{zn} - L_g)$
Time equation	$Et = 9.87 \sin 2\xi - 7.53 \cos\xi - 1.5 \sin\xi$ $\xi = 2\pi(n-1)/364$
Solar beam angle to west Solar beam angle to south	$W = \cos^{-1}(\cos\delta \times \sin H)$ $S = \cos^{-1}(1 - \cos^2 Z - \cos^2 W)^{1/2}$ Take the negative value of the root if, $\cos H < \tan\delta / \tan L$
Solar azimuth angle	If $\cos H > \tan\delta / \tan L$ $\phi = \sin^{-1}[\cos W / \cos(\pi/2 - Z)]$ If $\cos H < \tan\delta / \tan L$ $\phi = \pi - \sin^{-1}[\cos W / \cos(\pi/2 - Z)]$
Solar plan azimuth angle	$\gamma = \phi - \psi$